GDCh Research Article Angewandte International Edition Chemie www.angewandte.org

How to cite: *Angew. Chem. Int. Ed.* **2024**, *63*, e202411752
doi.org/10.1002/anie.202411752

Cluster Compounds

Strain-Induced Structural Rearrangement Towards a White-Light-Emitting Adamantane-Type Cluster Dimer

*Jie Wang, Iran Rojas-Leon, Niklas Rinn, Lukas Guggolz, Ferdinand Ziese, Simone Sanna, Nils W. Rosemann, and Stefanie Dehnen**

Dedicated to Prof. Dr. Wolfram Koch on the occasion of his 65th birthday

Abstract: Group 14/16 adamantane-type hybrid clusters of the type $[(RT)_4E_6]$ (T = group 14 element, E = group 16 element, R = organic group) have been reported to emit white-light when irradiated in an amorphous state with a continuous-wave (CW) infrared laser diode. This effect is enhanced if the cluster core is varied from a binary to a more complex composition. To further explore this phenomenon, we synthesized clusters with a multinary R/R'-T/T'-E/E' composition, including isolobal replacement of E with CH_2, in $[(2\text{-NpSi})\{CH_2Sn(S)Ph\}_3]$ (**1**, Np = naphthyl). When expanding one of the CH_2 moieties to a C_2H_4 group, thus generating a R/R'-T/T'-E/E'/E'' cluster composition, we unexpectedly observed a dimerization of the initially formed, yet non-isolable adamantane-like cluster $[(2\text{-NpSi})\{CH_2Sn(S)Ph\}\{C_2H_4Sn(S)Ph\}]$ (**2**) to $[(2\text{-NpSi})\{CH_2Sn(S)Ph\}_2\{C_2H_4Sn(S)Ph\}]_2$ (**3**), exhibiting a heretofore unprecedented cluster architecture. Both monomeric **1** and dimeric **3**, show white-light emission as thin films. The nonlinear optical response of the compounds was also modelled with DFT methods.

[*] M. Sc. J. Wang, Dr. I. Rojas-Leon, Dr. N. Rinn, Dr. L. Guggolz, Prof. Dr. S. Dehnen
Institute of Nanotechnology
Karlsruhe Institute of Technology
Kaiserstrasse 12, 76131 Karlsruhe, Germany.
E-mail: stefanie.dehnen@kit.edu

M. Sc. F. Ziese, Prof. Dr. S. Sanna
Institute of Theoretical Physics and Center for Materials Research (LaMa)
Justus Liebig University Giessen
Heinrich-Buff-Ring 16, 35392, Giessen, Germany

Dr. N. W. Rosemann
Light Technology Institute
Karlsruhe Institute of Technology
Kaiserstrasse 12, 76131 Karlsruhe, Germany

Introduction

Group 14/16 hybrid clusters based on $\{RTE_3\}$ fragments (T=Si, Ge, Sn; E=S, Se, Te; R = organic substituent) are accessible with a variety of structural motifs and correspondingly varying properties.[1–4] Studies of their chemical behavior addressed the reactivity and extension of the binary T–E cluster core to ternary ones exhibiting an M–T–E elemental combination (M = d-block metal)[5–9] as well as derivatization of the organic substituents on the binary or (extended) ternary cluster cores.[10–13] A common structural motif is the adamantane-type cluster of the general composition $[(RT)_4E_6]$, which has been known since the beginning of the last century[14] and has been reported with nearly all combinations of T and E and a wide variety of organic or organometallic substituents in the meantime.[10,15–18] While some of these compounds form crystals that have been structurally characterized, other compounds are either less prone to crystallization or do not form crystals at all. It was recently shown that such inherently amorphous materials like $[(StySn)_4S_6]$ (Sty = styryl)[19] and $[(PhT)_4S_6]$[20] (Ph = phenyl; T = Ge, Sn) can exhibit extreme non-linear optical properties, being able to convert near-infrared light from a continuous wave (CW) laser diode to directed white-light covering the whole visible range of the spectrum.[21,22] Detailed studies indicated that the habitus of the material indeed plays a major role, as the white-light emission can only occur in amorphous systems, while (nano)crystalline samples display intense second harmonic generation (SHG) instead.[7,20,21] Another precondition for the white-light emission seems to be the presence of an electron-rich (cyclic) organic substituent.[20,21] Consequently, other compounds, such as $[(MeSn)_4S_6]$ or $[(BuSn)_4S_6]$, show SHG even when in an amorphous state.[20] The T–E composition of the cluster core can also affect the optical properties by a spectral shift of the emitted light, which opened up the possibility to adjust the optical properties to any desired application. Such nonlinear optical phenomena were also observed for purely organic adamantanes $(RC)_4(CH_2)_6$,[23] which further increased the range of possible chemical variations, and with this, the range of options to fine tune the emitted spectra.[24–26]

Intrigued by the possibility to tailor the opto-electronic properties of adamantane-type compounds, and at the same time aiming at altering their processability, we sought to create adamantanes with mixed inorganic-organic cluster

cores. This was achieved by a multistep synthesis of compounds [(PhSi){CH_2Sn(E)Ph}$_3$] (E=S (**A**), Se, Te),[27] which indeed turned out to be transferrable without decomposition from the crystalline state to a glass-like state by congruent melting and subsequent cooling. The lack of long-range order ultimately allowed the glassy materials to exhibit white-light emission. Quantum chemical studies suggest that an increasing variation of the clusters, in terms of different T/T' and E/E' combinations is not only beneficial for their mechanical properties and processability, but also enhances the nonlinear optical response.[27] These encouraging results prompted us to additionally investigate the influence of a combination of different bridging ligands E/E' and also different substituents R/R' on chemical and optical properties. We chose to combine Np and Ph substituents (Np = naphthyl), which were previously shown to behave differently in terms of white-light emission versus SHG,[20] and to combine different bridging alkylene groups, ultimately leading to an R/R'-T/T'-E/E'/E''-style cluster variant.

Herein we report success of this approach by the synthesis of [(2-NpSi){CH_2Sn(S)Ph}$_3$] (**1**) and, upon modification of early steps of the synthesis, the even more unsymmetric cluster [(2-NpSi){CH_2Sn(S)Ph}$_2${C_2H_4Sn(S)Ph}] (**2**). In addition to the effect of the Np group on the electronic structure, we could show that the corresponding precursor can undergo a CH_2 insertion to from an unsymmetrical cluster (**2**), in which the steric demand of the new {C_2H_4} group causes a heretofore unprecedented, but energetically preferred, dimerization of **2**. This afforded the unique dimeric cluster [(2-NpSi){CH_2Sn(S)Ph}$_2${C_2H_4Sn(S)Ph}]$_2$ (**3**) over time, as monitored and studied by NMR spectroscopy and density functional theory (DFT) calculations, and as finally confirmed by single-crystals. The nonlinear optical response of the compounds was explored spectroscopically and also modelled with DFT-based methods in the time-domain. The calculations predict a high 2nd order non-linear response for compound **2**, while two conformers of compound **3** (denoted as **3A** and **3B**) that differ by rotation of the organic groups, display a much lower, nearly identical optical non-linearity.

Results and Discussion

Syntheses and Crystal Structures

To obtain the desired adamantane-like clusters, we followed a synthesis route similar to a reported one.[27] 2-NpSiCl_3 served as the precursor in an insertion reaction using $BrCH_2Cl$ and *n*-BuLi to obtain 2-NpSi(CH_2Cl)$_3$ (**1a**; Scheme 1). Increasing the concentration of both reagents resulted in the insertion of another CH_2 moiety to form an ethylene group in 2-NpSi(CH_2Cl)$_2$(C_2H_4Cl) (**2a**). This reactivity was not observed in the corresponding phenyl-decorated silane. Next, both compounds were stannylated by addition of Ph_3SnNa, resulting in 2-NpSi(CH_2SnPh_3)$_3$ (**1b**) and 2-NpSi(CH_2SnPh_3)$_2$($C_2H_4SnPh_3$) (**2b**). Subsequent substitution of the terminal phenyl groups with Cl using hydrochloric acid afforded the cluster precursors 2-NpSi{CH_2Sn(Ph)Cl_2}$_3$ (**1c**) and 2-NpSi{CH_2Sn(Ph)Cl_2}$_2${C_2H_4Sn(Ph)Cl_2} (**2c**). In the final step, these were reacted with ($SiMe_3$)$_2$S to form the target compounds [(2-NpSi){CH_2Sn(S)Ph}$_3$] (**1**) and [(2-NpSi){CH_2Sn(S)Ph}$_2${C_2H_4Sn(S)Ph}] (**2**) in a condensation reaction. For experimental details as well as analytical data of all compounds as well as single-crystal data of compounds **1b**, **1c**, **1**, **2b**, and **3**, see the Supporting Information.[28]

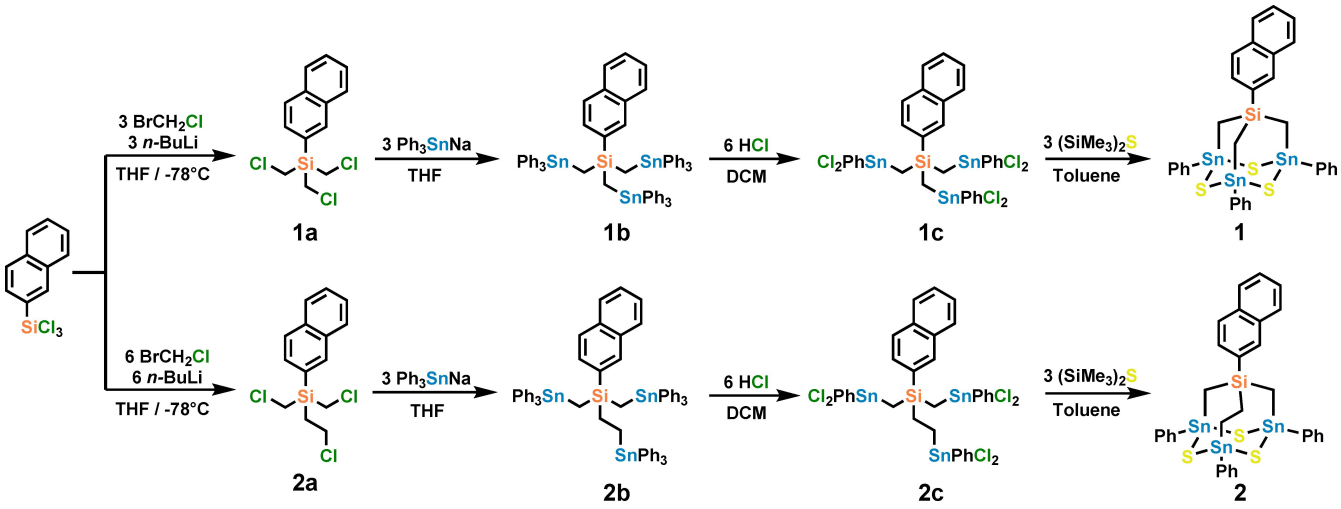

Scheme 1. Illustration of the synthesis pathway towards organometallic adamantane-based clusters [(2-NpSi)(CH_2Sn(S)Ph)$_3$] (**1**) and [(2-NpSi){CH_2Sn(S)Ph}$_2${C_2H_4Sn(S)Ph}] (**2**). Side products are omitted for clarity. The adamantane-type cluster **1**, which represents the Np-substitute of previously reported [(PhSi){CH_2Sn(S)Ph}$_3$] (**A**),[27] consist of a quaternary {Si(CH_2)$_3$Sn$_3$S$_3$} adamantane-type core decorated by one naphthyl and three phenyl groups. It was characterized by NMR and IR spectroscopy as well as via ESI-MS. The crystal structure of **1** was determined by X-ray diffraction of single crystals, which were grown by layering a solution of **1** in THF with *n*-hexane. Cluster 2 was identified by means of spectrometric and spectroscopic methods.

1 crystallizes in the monoclinic crystal system (space group $P2_1/c$) with one molecule per asymmetric unit and four molecules per unit cell. The adamantane-type scaffold was confirmed as being based on a $\{(PhSn)_3S_3\}$ six-membered ring in chair-type conformation, which is capped by a $\{(2\text{-NpSi})(CH_2)_3\}$ fragment via three C–Sn bonds. A comparison with the structure of **A** (Figure 1) indicates a very similar cluster core, with the largest difference being the slightly smaller $Si–C_{CH2}$ distances in **1** (1.854(6)–1.858(5) Å) as compared to those in **A** (1.868(6)–1.943(6) Å) (see Table 1).

In contrast, crystals of compound **2** could not be obtained in any of our experiments, so an exact structural study could not be carried out by experimental techniques. However, we were able to detect the cluster by mass spectrometry, as the ESI^+ mass spectrum revealed signals for $[\mathbf{2}+Cl]^-$ at m/z 929.803 with the characteristic isotopic pattern (Figure S44). In addition, we computed the energetic minimum structure of the molecule by using the program system TURBOMOLE[29] and applying DFT methods,[29–34] denoted as $\mathbf{2}^{calc}$ (Figure 2). While the overall structure is very similar to **1** and **A**, the bonding and the dihedral angles in the cluster core indicate an increased distortion in $\mathbf{2}^{calc}$, as a consequence of the presence of the ethylene bridge (see Table 1).

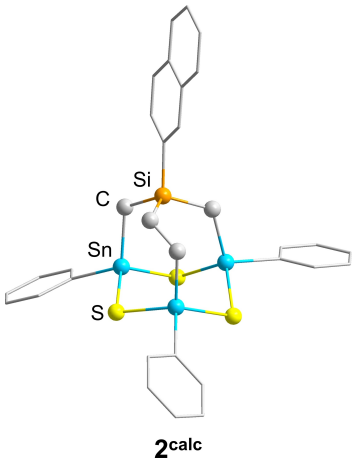

$\mathbf{2}^{calc}$

Figure 2. Computed energetic minimum structure of the cluster molecule $\mathbf{2}^{calc}$. Hydrogen atoms are omitted for clarity. Structural parameters are summarized in Table 1.

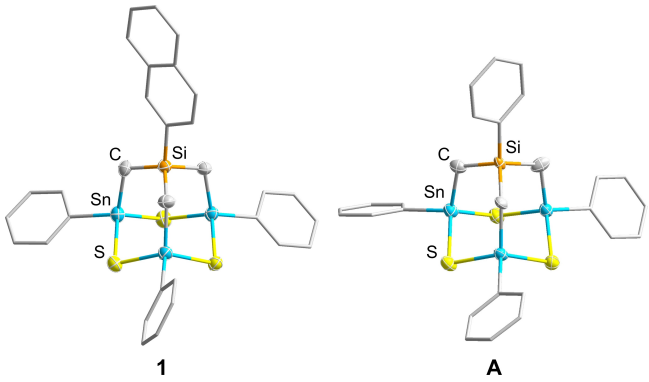

1 **A**

Figure 1. Molecular structure of the adamantane-type clusters **1** and the previously published compound $[(PhSi)(CH_2Sn(S)Ph)_3]$ **A** with ternary inorganic scaffolds. Ellipsoids are displayed at 50% probability and hydrogen atoms are omitted for clarity. Structural parameters are summarized in Table 1.

By inspection of ^1H and ^{119}Sn spectra, we detected a second set of peaks, belonging to an unknown species, denoted as compound **3** (Figure 3, top). When repeating the NMR experiments after four weeks on the same sample, the spectra lacked any signals of **2**, with only the peaks of **3** remaining (Figure 3, bottom). While this was noticeable in the ^1H NMR spectra as well, it was even more clearly observed in the ^{119}Sn NMR data due to more distinct peak separation: directly after addition of $(SiMe_3)_2S$ to **2c**, two signals are observed at 85.7 and 78.7 ppm in a 2:1 ratio, stemming from the Sn atoms of **2** connected to methylene and ethylene moieties, respectively. However, signals of **3** are already predominant, appearing at 92.8 and 99.7 ppm in

Table 1: Experimental structural parameters of $[(2\text{-NpSi})\{CH_2Sn(S)Ph\}_3]$ (**1**), $[(PhSi)\{CH_2Sn(S)Ph\}_3]$ (**A**)[27] and $[(2\text{-NpSi})\{CH_2Sn(S)Ph\}_2\{C_2H_4Sn(S)Ph\}_2]$ (**3**), as well as the computational data (DFT) for calculated $[(2\text{-NpSi})\{CH_2Sn(S)Ph\}_2\{C_2H_4Sn(S)Ph\}]$ ($\mathbf{2}^{calc}$) for comparison.

Distance/ Angle	1 [Å/°]	A [Å/°]	$\mathbf{2}^{calc}$ [Å/°]	3 [Å/°]
$Si–C_{Np/Ph}$	1.872(6)	1.834(7)–1.876(5)	1.896	1.886(5)
$Si–C_{CH2}$	1.854(5)–1.859(5)	1.868(6)–1.943(6)	1.877–1.889	1.857(5)–1.869(6)
$Si–C_{(C2H4)}$	–	–	1.906	1.874(5)
Sn–S	2.395(2)–2.424(2)	2.395(2)–2.428(2)	2.426–2.4442	2.394(1)–2.409(2)
$Sn–C_{CH2}$	2.130(5)–2.151(5)	2.127(7)–2.159(7)	2.175–2.111	2.124(5)–2.142(5)
$Sn–C_{C2H4}$	–	–	2.184	2.151(5)
$Sn–C_{Ph}$	2.123(5)–2.149(5)	2.114(5)–2.139(7)	2.152–2.154	2.126(5)–2.136(6)
$C_{CH2}–Si–C_{CH2}$	107.8(2)–111.5(2)	108.1(2)–110.9(2)	110.9	110.5(3)
$C_{CH2}–Si–C_{C2H4}$	–	–	109.4–113.2	108.9(2)–113.0(3)
$Si–C_{CH2}–Sn$	118.0(3)–118.1(3)	116.5(3)–119.0(3)	116.5–124.5	117.0(3)–120.6(3)
$C_{CH2}–Sn–S$	108.1(2)–111.6(2)	107.3(2)–114.7(1)	106.1–112.9	109.0(2)–114.1(2)
$C_{C2H4}–Sn–S$	–	–	109.3–110.9	103.1(2)–104.0(2)
S–Sn–S	109.50(5)–111.14(5)	104.57(5)–111.02(5)	110.3–113.7	107.58(5)–115.53(5)
Sn–S–Sn	98.57(5)–98.86(5)	97.65(6)–99.29(5)	96.9–106.9	98.62(5)–109.49(6)

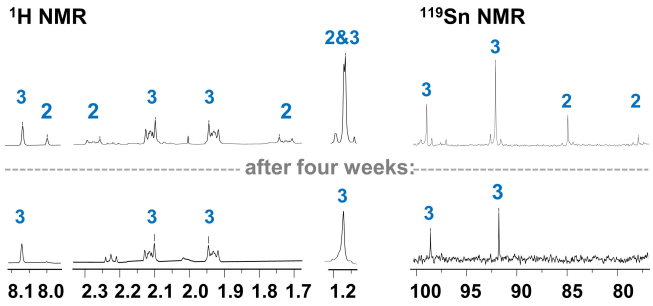

Figure 3. ^{1}H NMR spectra (left) and ^{119}Sn NMR spectra (right) of the reaction solutions of 2-NpSi(SnPhCl$_2$)$_3$ (**2c**) and (SiMe$_3$)$_2$S directly after begin of the reaction (top) or four weeks later (bottom). Signals for **2** and **3** are assigned.

the same 2:1 ratio. The disappearance of the former signals after four weeks indicated full conversion of **2** to **3** over time.

Compound **3** crystallizes in the orthorhombic crystal system (space group *Pbca*) with half a formula unit per asymmetric unit and four formula units per unit cell. The asymmetric unit consists of a {2-NpSi(CH$_2$)$_2$(PhSn)$_2$S} unit based on a {SiC$_2$Sn$_2$S} six-membered ring in chair conformation, the Sn atoms of which are bridged by another {S$_2$SnPh} moiety that is additionally connected to a bridging C$_2$H$_4$ group. The latter connects this asymmetric unit to an identical, yet inverted unit via a C–Si bond. This way, a dimeric, inversion-symmetric scaffold is generated. It is based on a fourteen-membered {SnSSnCSiC$_2$}$_2$ macrocycle that is expanded by two {(PhSn)S$_2$C} units on each side to form a tricyclic arrangement. Formally, this motif can be described as two molecules of **2**, each of which have exchanged an intramolecular Sn–C$_2$H$_4$–Si bridge for an intermolecular one. As a consequence, a structural rearrangement occurred leading to a twisted-boat conformation of the {Sn$_3$S$_3$} six-membered ring that occurred in chair conformation in the structures of **1** and **A** (and in the computed structure of **2**^{calc}). Figure 4 illustrates the molecular structure of the cluster dimer **3**. An overview of the structural parameters in compounds **1**, **A**, **2**^{calc}, and **3** is given in Table 1. While most of the structural parameters (in particular the distances) are very similar, S–Sn–S and C–Sn–S angles exhibit a slightly greater variety in **3** as compared to the adamantane-type clusters. The largest deviation is observed for the Sn–S–Sn angles, where the maximum in **1** is surpassed by 10° in the structure of compound **3**. This is due to the conformational change of the {Sn$_3$S$_3$} six-membered ring from chair to twisted-boat conformation, which obviously facilitates accommodating the intermolecular ethylene bridge.

The calculated structure of **2** exhibits distortions due to the ethylene group being incorporated, resulting in larger variations of most of the bond angles as compared to **1** and **A**, while compound **3** allows for some relaxation. The degree of distortion was quantified by comparing the deviations of the measures of the trigonal pyramids defined by the three S atoms and the Si atom of (computed) clusters **1**, **2**, and **3** from that of an ideal tetrahedron with the same

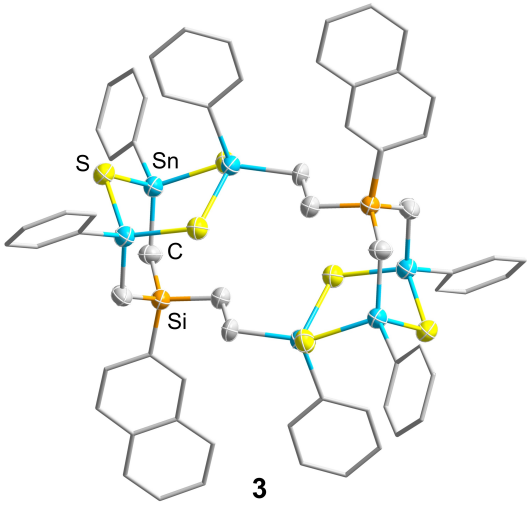

Figure 4. Molecular structure of the cluster dimer **3**. Thermal ellipsoids are displayed at 50% probability; hydrogen atoms are omitted for clarity. Structural parameters are summarized in Table 1.

volume as the pyramid in **1**. The mean deviation d_j (j=0–3) of the atomic coordinates $r_i^{(j)}$ (i=1–4) of the corners of the discussed pyramids, thus of $r_i^{(1)}$ of compound **1**, of $r_i^{(2)}$ of compound **2**, and of $r_i^{(3)}$ of compound **3** from the corners $r_i^{(0)}$ of an ideal tetrahedron possessing the volume of the pyramid in compound **1** are given as shown in equation (1):

$$d_j = \frac{1}{4}\sum_i \left| r_i^{(j)} - r_i^{(0)} \right| \quad (1)$$

Using the calculated coordinates, one obtains the following values, d_1=0.243 Å, d_2=0.388 Å, d_3=0.254 Å, d_0=0.000 Å, confirming the largest deviation to occur for cluster **2**. We therefore hypothesize that by forming **3**, the system escapes the tension that an ethylene bridge appears to introduce into the architecture of the adamantane-like cluster (Scheme 2). Computational studies using DFT methods showed the dimerization to be exoenergetic by −33 kJ/mol (see Supporting Information for details). The formation of intermediate **2** thus seems to occur due to the kinetically favorable intramolecular ring formation at an isolated **2c** molecule, as opposed to the dimerization requiring two **2c** units. For comparison, and to understand the isolation of **1** instead of an analogous dimer, we computed the hypothetical dimerization of **1**, too. The DFT calculations converged into a minimum structure (**1**$^{dimer-calc}$, see Figure S61), but the corresponding reaction energy of +34 kJ/mol indicates an endoenergetic process. This suggests that this reaction does not take place, in agreement with the experimental observations.

When isolated from the reaction without a preceding layering step, compounds **1** and **3** are obtained in a mainly amorphous state, with some signs of (micro)crystallinity, as confirmed by the PXRD analyses (Figures S53 and S56), but can be converted to a single-crystalline form by re-dissolving and layering as described above. Given this control of the habitus, we aimed at exploring potential nonlinear optical

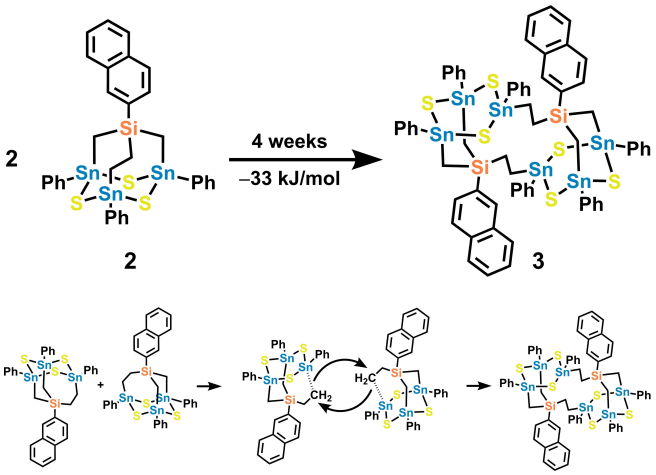

Scheme 2. Top: Reaction scheme illustrating the experimentally observed and quantum chemically modelled transformation of the multinary adamantane-type cluster [(2-NpSi){$CH_2Sn(S)Ph$}$_2${$C_2H_4Sn(S)Ph$}] (**2**) into its dimer [(2-NpSi){$CH_2Sn(S)Ph$}$_2${$C_2H_4Sn(S)Ph$}]$_2$ (**3**). Bottom: Suggestion for the concerted mutual attack of two appropriately oriented cluster molecules initiating the substitution reaction during the dimerization.

properties of these compounds, which is described in the following section.

Nonlinear Optical Response

For characterizing the nonlinear response of **1** and **3**, thin films of the powder samples were prepared by pulsed laser deposition (PLD). For further information on the PLD process, see the Supporting Information (Figure S45).

The thin-film samples were transferred to the optical setup and the sample chamber was evacuated to static pressure below 1×10^{-4} mbar. For excitation, a continuous-wave (CW) laser diode operating at 980 nm (1.26 eV) was used. We note in passing that the photon energy of the laser is far below the band gap energy of the material that is found to be ~4 eV for both compounds (see Figure S64).

The emitted light was focused and relayed onto the entrance slit of a CCD-based compact spectrometer (Ocean-Optics HR2000). To block residual excitation light from entering the spectrometer, a two-coloured bandpass filter (KG3, 2 mm thickness) was used. To compensate for the absorption of the filter, the throughput of the whole optical system was corrected using a calibrated tungsten halogen lamp.

For both compounds, white-light emission with a warm-white colour impression is observed upon an inexpensive treatment with the CW laser diode. This emission differs significantly from the emission observed when exciting the compounds with photon energies above the band gap, i.e., the standard linear response observed as photoluminescence (see Figure S64), This emphasizes the extraordinary nonlinear character of the observed white-light emission, which is the primary focus and motivation of our studies.

Similar white-light emission spectra are found for various laser thresholds depending on the sample position. This behaviour is most likely attributed to an inhomogeneous film-thickness over the sample, which is comparable with the unordered situation in an amorphous powder. The inherent inhomogeneity of the films also inhibits a quantitative analysis of the white-light emission efficiency, so we will focus on the qualitative findings.

Exemplary emission spectra are shown in Figure 5a. The depicted spectra were recorded using an excitation density of 1300 W/cm^2 and 300 W/cm^2 for **1** and **3**, respectively. For both samples the emission spectrum rises continuously towards the available detection window. In Figure 5b, the emission spectra are converted using the 1931 CIE photopic luminosity function. The resulting spectra give an understanding of the emissions' color impression. For both samples, the spectra peak at ~600 nm, which is in perfect agreement with the perceived warm-white color.

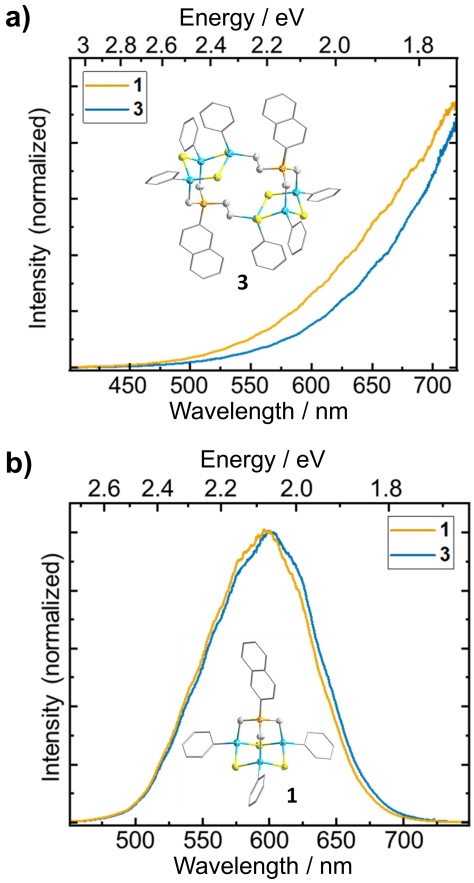

Figure 5. a) Emission spectrum of **1** (orange line) and **3** (blue line) following 980 nm excitation; for comparison the spectra are normalized to the same intensity at 730 nm; the inset depicts the molecular structure of cluster dimer **3**. b) Emission spectrum of **1** (orange line) and **3** (blue line) following 980 nm excitation, plotted as photometric spectrum, i.e., as perceived under photopic vision, to convey the colour impression (see main text for details); the inset depicts the molecular structure of cluster **1**.

Computational Studies of the SHG Response

As both compounds, thus one based on a monomeric cluster lacking inversion symmetry (**1**) and one based on a dimeric cluster possessing an inversion center (**3**), exhibit a similar nonlinear response in the form of WLG, we were interested to explore whether their molecular symmetry would affect the nonlinear optical response in general. WLG requires an as yet undefined addition of various higher-order contributions to the nonlinear optical response, which cannot be easily quantified. We therefore performed theoretical investigations of the SHG response, although we found the SHG to not be experimentally accessible because of the dominance of the WLG signal.

The computations of compounds **1**, **2**, **3**, and **A** were conducted with periodic boundary conditions (hence on 'crystals') using the Yambo software package for the calculation of SHG spectra in the real-time approach and within the independent particle approximation.[35] The corresponding structures have been optimized until the Hellmann-Feynman forces acting on the single atoms were lower than 0.005 eV/Å. The forces were calculated within DFT using VASP PAW-PBE with the DFT–D3 method with BJ damping for vdW interactions.[36–41]

The computed SHG response of the crystalline compound **2**, as compared to that of **A** and **1**, is shown in Figure 6. It is similar to that observed for other monomeric or aggregated structures, such as the homogeneous and heterogeneous dimers, or crystalline species inheriting the characteristic of the parent molecules. The SHG spectra of **A**, **2**, and **1** depicted in Figure 6 thus feature signatures at similar energies, yet with slightly differing intensity. The first spectroscopic signature occurs at 1.8 eV. While it is a pronounced peak for **2**, it is no more than a shoulder for compound **A**. The intensities are predicted to be rather similar for the investigated clusters also at higher energies, again with slightly differing absolute value. The signature of **1** exhibits an intensity between **2** and **A** in the lower-energy region (<2.5 eV). In all three cases, the first major peak is located at roughly half of the calculated energy of the HOMO–LUMO gap, which is in agreement with the findings for other optically nonlinear cluster compounds with different substituents,[7,22,27,42,43] and could be therefore considered as another precondition for the observed phenomena.

Further analyses of the charge densities demonstrate that the electronic transitions giving rise to the first peak of compound **2** at 1.8 eV occur between occupied and empty electronic states originating from the naphthyl electronic levels, and are therefore spatially localized on the substituents. In Figure 7, the intersection of occupied orbitals and unoccupied orbitals (marked in orange in the energy level Scheme) is demonstrated to be located at the Np groups.

In the computations with periodic boundary conditions, we found two slightly different local minimum structures for compound **3**, denominated as species **3A** and **3B** (see Figures S62 and S63), in which the organic substituents are rotated in different directions. The structural parameters of both of these conformers are in good agreement with those of $\mathbf{3}^{\mathbf{calc}}$ and of the experimental structure of **3**. The bond lengths differ by 10^{-3} Å at the maximum. Past investigations of (monomeric) adamantane-based clusters with organic substituents suggested that the energy barrier for rotation of the organic groups on the group 14 element for these structures is low,[42] suggesting that **3 A** is easily dynamically transformed in 3B and vice-versa. However, the two minimum structures also exhibit a notable difference in the magnitude of their deviation from the inversion symmetry. The deviation from the inversion symmetry was defined by

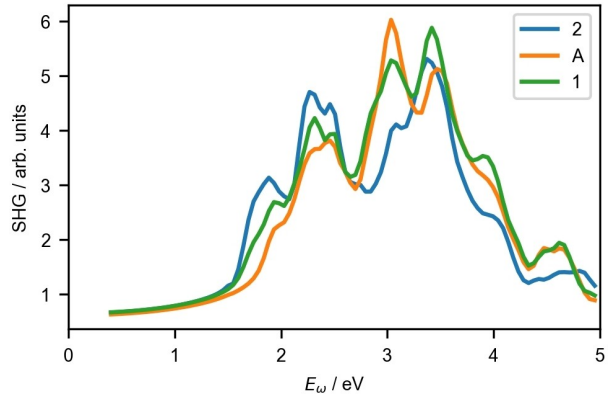

Figure 6. SHG response averaged over all directions of **A**, **1**, and **2** calculated within DFT in the independent particle approximation.

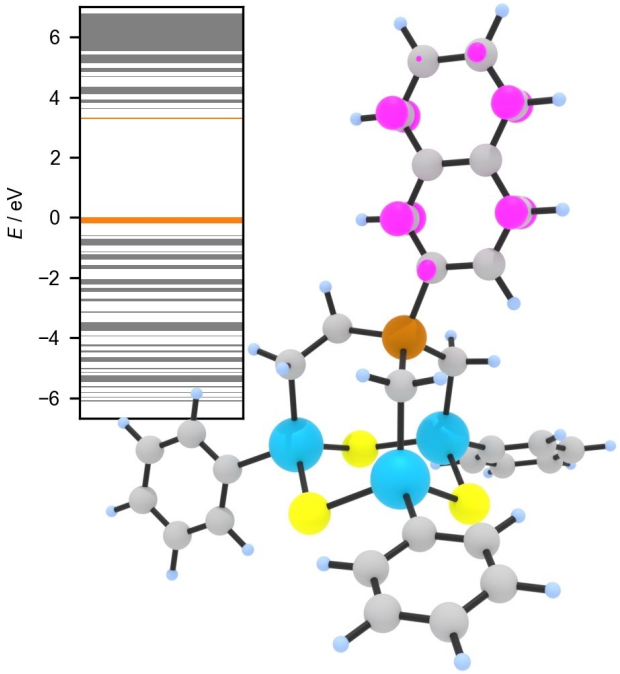

Figure 7. Computed overlap (pink, right hand side) of the highlighted unoccupied and occupied orbital groups (orange, left hand side). Energy levels are given within a delta of 0.1 eV. The overlap is clearly located on the Np substituents. The colour code of the atoms is the same as in Figures 1, 2, 4, and 5.

the tolerance (in Å) needed for the structure to be perfectly symmetric (Table 2).

Still, the magnitude of the deviation from inversion symmetry is very low in both cases, and suggests that the SHG response should be quenched.[44] This is indeed the case, as demonstrated in Figure 8, which shows the calculated SHG response of compounds **2**, **3 A**, and **3B**. The intensities of **3 A** and **3B** represent the limit of the numerical accuracy of our computational approach, essentially meaning no SHG response. Although the deviation from inversion symmetry of compounds **3 A** and **3 B** differs by two orders of magnitude, the magnitude of the SHG coefficients is nearly identical. This might be due to the fact that both compounds are below a symmetry threshold under which we cannot resolve any difference, and the SHG signal effectively vanishes. Another explanation might be related to the fact that the charge distribution has a higher symmetry than the atomic structure.

Conclusion

We have introduced a 2-naphthyl group to our previously described adamantane-type clusters and observed the impact on structure and optical properties of the product **1**. The addition of further equivalents of $BrCH_2Cl_2$ during the synthesis introduced an ethylene bridge in the adamantane cluster **2**. The thus introduced higher strain in the cage compound prompted a dimerization to form cluster **3**, affording an unprecedented macrocycle. This compound also shows white-light generation in its amorphous habitus and the SHG behavior of the compounds was investigated in a theoretical study. The exact formation mechanism of **3** from **2** is currently investigated within our research group. We will also try to introduce further (poly)aromatic substituents to the system to investigate the optical impact as well as the influence on the inclusion of multiple CH_2 groups during the formation. Previous computational studies showed that the habitus and composition of different cluster materials, including mixtures of different (separate) molecules, is accompanied by different aggregation modes of nearest neighbors. Hence, future investigations will include studies on how other dimers analogous to compound **3**, and also dimers consisting of two different monomers can influence the SHG intensity and the inheritance of characteristics from a given monomeric counterpart in such mixtures.

Table 2: Deviation from perfect inversion symmetry of the calculated structures **3 A** and **3B**.

Species	Tolerance [Å]
3 A	1.3×10^{-3}
3B	5.0×10^{-5}

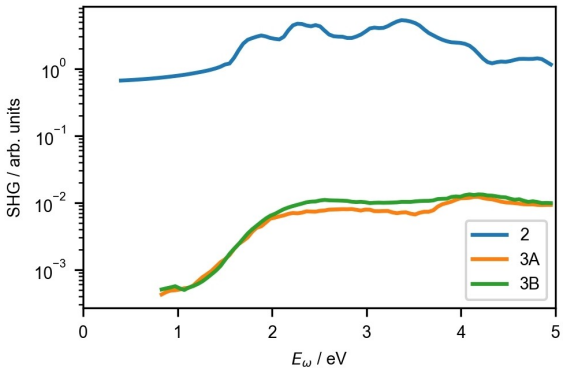

Figure 8. SHG response on a logarithmic scale, averaged over all directions of compound **2**, **3 A**, and **3B**, as calculated by DFT methods within the independent particle approximation. We can observe that the SHG intensity is quenched by 2–3 orders of magnitude by introducing (approximate) inversion symmetry in **3 A** and **3B** as compared to the monomeric 'parent' cluster **2**. For the sake of clarity, the signals are smoothed by plotting the rolling mean.

Supporting Information

The authors have cited additional references within the Supporting Information.[45–52]

Acknowledgements

This work was supported by the Deutsche Forschungsgemeinschaft within the framework of the research group FOR2824 (Grant No. 398143140). The authors acknowledge support by the state of Baden-Württemberg through bwHPC and the German Research Foundation (DFG) through grant no INST 40/575-1 FUGG (JUSTUS 2 cluster) and by the Karlsruhe Nano Micro Facility (KNMFi). Calculations for SHG response were conducted on the Lichtenberg high-performance computer of Technical University Darmstadt as well as at the Höchstleistungsrechenzentrum Stuttgart (HLRS). We further acknowledge computational resources provided by the HPC Core Facility and the HRZ of the Justus-Liebig-Universität Giessen. Open Access funding enabled and organized by Projekt DEAL.

Conflict of Interest

The authors declare no conflict of interest.

Data Availability Statement

The data that support the findings of this study are available from the corresponding author upon reasonable request.

Keywords: multinary adamantane-type clusters · dimerization · single-crystal X-ray diffraction · non-linear optical properties · DFT studies

[1] W. Ando, T. Kadowaki, Y. Kabe, M. Ishii, *Angew. Chem. Int. Ed. Engl.* **1992**, *31*, 59–61.
[2] Z. Hassanzadeh Fard, C. Müller, T. Harmening, R. Pöttgen, S. Dehnen, *Angew. Chem. Int. Ed.* **2009**, *48*, 4441–4444.
[3] Z. H. Fard, M. R. Halvagar, S. Dehnen, *J. Am. Chem. Soc.* **2010**, *132*, 2848–2849.
[4] J. Keuter, K. Schwedtmann, A. Hepp, K. Bergander, O. Janka, C. Doerenkamp, H. Eckert, C. Mück-Lichtenfeld, F. Lips, *Angew. Chem. Int. Ed.* **2017**, *56*, 13866–13871.
[5] E. Leusmann, N. W. Rosemann, B. Weinert, S. Chatterjee, S. Dehnen, *Eur. J. Inorg. Chem.* **2016**, *2016*, 5300–5304.
[6] N. Rinn, L. Guggolz, J. Lange, S. Chatterjee, T. Block, R. Pöttgen, S. Dehnen, *Chem. Eur. J.* **2018**, *24*, 5840–5848.
[7] E. Dornsiepen, F. Dobener, N. Mengel, O. Lenchuk, C. Dues, S. Sanna, D. Mollenhauer, S. Chatterjee, S. Dehnen, *Adv. Opt. Mater.* **2019**, *7*, 1801793.
[8] B. Peters, N. Lichtenberger, E. Dornsiepen, S. Dehnen, *Chem. Sci.* **2020**, *11*, 16–26.
[9] R. Hauser, K. Merzweiler, *Z. Anorg. Allg. Chem.* **2002**, *628*, 905.
[10] K. Merzweiler, H. Kraus, *Z. Naturforsch. B* **1994**, *49*, 621–626.
[11] M. Unno, Y. Kawai, H. Shioyama, H. Matsumoto, *Organometallics* **1997**, *16*, 4428–4434.
[12] J. J. Vittal, *Polyhedron* **1996**, *15*, 1585–1642.
[13] J. R. Stellhorn, S. Hayakawa, B. D. Klee, B. Paulus, J. Link Vasco, N. Rinn, I. Rojas León, C. A. Hosier, S. Dehnen, W. Pilgrim, *Adv. Opt. Mater.* **2023**, *11*, 2201932.
[14] P. Pfeiffer, L. Rügheimer, *Ber. Dtsch. Chem. Ges.* **1903**, *36*, 3027–3030.
[15] J. A. Forstner, E. L. Muetterties, *Inorg. Chem.* **1966**, *5*, 552–554.
[16] R. H. Benno, C. J. Fritchie, *J. Chem. Soc. Dalton Trans.* **1973**, 543.
[17] M. Unno, D. Ishii, H. Matusmoto, *B. Chem. Soc. Jpn.* **1999**, *72*, 2469–2473.
[18] A. Blecher, M. Dräger, B. Mathiasch, *Z. Naturforsch. B* **1981**, *36*, 1361–1367.
[19] N. W. Rosemann, J. P. Eußner, A. Beyer, S. W. Koch, K. Volz, S. Dehnen, S. Chatterjee, *Science* **2016**, *352*, 1301–1304.
[20] N. W. Rosemann, J. P. Eußner, E. Dornsiepen, S. Chatterjee, S. Dehnen, *J. Am. Chem. Soc.* **2016**, *138*, 16224–16227.
[21] E. Dornsiepen, F. Dobener, S. Chatterjee, S. Dehnen, *Angew. Chem. Int. Ed.* **2019**, *58*, 17041–17046.
[22] S. Dehnen, P. R. Schreiner, S. Chatterjee, K. Volz, N. W. Rosemann, W. Pilgrim, D. Mollenhauer, S. Sanna, *ChemPhotoChem* **2021**, *5*, 1033–1041.
[23] S. Gowrisankar, C. A. Hosier, P. R. Schreiner, S. Dehnen, *ChemPhotoChem* **2022**, *6*, e202200128.
[24] N. W. Rosemann, H. Locke, P. R. Schreiner, S. Chatterjee, *Adv. Opt. Mater.* **2018**, *6*, 1701162.
[25] a) K. Hanau, S. Schwan, M. R. Schäfer, M. J. Müller, C. Dues, N. Rinn, S. Sanna, S. Chatterjee, D. Mollenhauer, S. Dehnen, *Angew. Chem. Int. Ed.* **2021**, *60*, 1176–1186; b) M. J. Müller, F. Ziese, J. Belz, F. Hüppe, S. Gowrisankar, B. Bernhardt, S. Schwan, D. Mollenhauer, P. R. Schreiner, K. Volz, S. Sanna, S. Chatterjee, *Opt. Mater. Express* **2022**, *12*, 3517; c) S. Schwan, A. J. Achazi, F. Ziese, P. R. Schreiner, K. Volz, S. Dehnen, S. Sanna, D. Mollenhauer, *J. Comput. Chem.* **2023**, *44*, 843–856.
[26] S. Gowrisankar, B. Bernhardt, J. Becker, P. R. Schreiner, *Eur. J. Org. Chem.* **2021**, *2021*, 6806–6810.
[27] a) J. Ayari, C. R. Göb, I. M. Oppel, M. Lutter, W. Hiller, K. Jurkschat, *Angew. Chem. Int. Ed.* **2020**, *59*, 23892–23898; b) I. Rojas-León, J. Christmann, S. Schwan, F. Ziese, S. Sanna, D. Mollenhauer, N. W. Rosemann, S. Dehnen, *Adv. Mater.* **2022**, *34*, 2203351.
[28] Deposition Numbers 2361682 (for **1b**), 2361683 (for **1c**), 2361684 (for **1**), 2361685 (for **2b**), and 2361686 (for **3**) contain the supplementary crystallographic data for this paper. These data are provided free of charge by the joint Cambridge Crystallographic Data Centre and Fachinformationszentrum Karlsruhe at http://www.ccdc.cam.ac.uk/structures.
[29] TURBOMOLE V7.7.1, a development of University of Karlsruhe and Forschungszentrum Karlsruhe GmbH, *TURBOMOLE GmbH,since 2007*, **2023**, DOI http://www.turbomole.com.
[30] K. Eichkorn, O. Treutler, H. Öhm, M. Häser, R. Ahlrichs, *Chem. Phys. Lett.* **1995**, *240*, 283–290.
[31] K. Eichkorn, F. Weigend, O. Treutler, R. Ahlrichs, *Theor. Chim. Acta* **1997**, *97*, 119–124.
[32] J. Tao, J. P. Perdew, V. N. Staroverov, G. E. Scuseria, *Phys. Rev. Lett.* **2003**, *91*, 146401.
[33] F. Weigend, *Phys. Chem. Chem. Phys.* **2006**, *8*, 1057.
[34] F. Weigend, R. Ahlrichs, *Phys. Chem. Chem. Phys.* **2005**, *7*, 3297.
[35] F. Weigend, M. Häser, H. Patzelt, R. Ahlrichs, *Chem. Phys. Lett.* **1998**, *294*, 143–152.
[36] E. Caldeweyher, C. Bannwarth, S. Grimme, *J. Chem. Phys.* **2017**, *147*, 034112.
[37] E. Caldeweyher, S. Ehlert, A. Hansen, H. Neugebauer, S. Spicher, C. Bannwarth, S. Grimme, *J. Chem. Phys.* **2019**, *150*, 154122.
[38] E. Caldeweyher, J.-M. Mewes, S. Ehlert, S. Grimme, *Phys. Chem. Chem. Phys.* **2020**, *22*, 8499–8512.
[39] C. Attaccalite, M. Grüning, *Phys. Rev. B* **2013**, *88*, 235113.
[40] G. Kresse, J. Furthmüller, *Comput. Mater. Sci.* **1996**, *6*, 15–50.
[41] G. Kresse, J. Furthmüller, *Phys. Rev. B* **1996**, *54*, 11169–11186.
[42] G. Kresse, J. Hafner, *Phys. Rev. B* **1993**, *47*, 558–561.
[43] G. Kresse, D. Joubert, *Phys. Rev. B* **1999**, *59*, 1758–1775.
[44] S. Grimme, S. Ehrlich, L. Goerigk, *J. Comput. Chem.* **2011**, *32*, 1456–1465.
[45] B. Metz, H. Stoll, M. Dolg, *J. Chem. Phys.* **2000**, *113*, 2563–2569.
[46] R. S. Mulliken, *J. Chem. Phys.* **1955**, *23*, 2338–2342.
[47] A. E. Reed, R. B. Weinstock, F. Weinhold, *J. Chem. Phys.* **1985**, *83*, 735–746.
[48] C. Ehrhardt, R. Ahlrichs, *Theor. Chim. Acta* **1985**, *68*, 231–245.
[49] S. F. Boys, in Quantum Theory of Atoms, Molecules and the Solid State (Ed.: P.-O. Löwdin), New York, 1966, 253–262.
[50] S. Grimme, J. Antony, S. Ehrlich, H. Krieg, *J. Chem. Phys.* **2010**, *132*, 154104.
[51] P. E. Blöchl, *Phys. Rev. B* **1994**, *50*, 17953–17979.
[52] K. Momma, F. Izumi, *J. Appl. Crystallogr.* **2011**, *44*, 1272–1276.

Manuscript received: June 22, 2024
Accepted manuscript online: August 19, 2024
Version of record online: October 22, 2024